ChemComm

COMMUNICATION

View Article Online
View Journal | View Issue

Cite this: *Chem. Commun.*, 2022, **58**, 5009

Received 17th February 2022,
Accepted 21st March 2022

DOI: 10.1039/d2cc00988a

rsc.li/chemcomm

Partial induced reorientation of 5CB in a liquid crystal microarray and a signal-on sensing assay for the detection of aflatoxin B1†

Shihong Wang, Ting Huang, Jun Zhou, Qianshan Chen,* Zhaoyang Wu * and Ruqin Yu

Herein, a signal-on liquid crystal microarray (LCM) sensor is designed for the first time with a micro-spectral optical sensing signal. Depending on the change of the orientation of the LC molecules in the LCM films and the intensity of the spectral peaks of the PhCs, the signal-on LCM biosensor achieves the detection of AFB1 and the Partial Response Mechanism (PSM) of the LCM films is discovered.

Liquid crystal (LC) sensors, using the LC as an optical signal element, have been researched extensively, particularly in the context of optical devices and the biosensor field.[1,2] Relying on the elasticity and birefringence of LC molecules, LC/aqueous sensing systems convert chemical signals into optical output signals *via* orientational transitions of the LC molecules,[3] and LC sensors can successfully report a series of biomolecular interactions and enzymatic events (*e.g.*, proteins,[4,5] phospholipids,[6] oligopeptides,[7,8] DNA,[9,10] and so on[11–13]). That is, in the presence of an external stimulus, the balance of LC orientation in the bulk, which depends on the nature of the surface or the interface of the LC films, is broken, and the long axis of the LC molecules turns to a homeotropic (perpendicular) or planar alignment.[14] Although these LC optical images caused by the long axis change of the LC molecules play a vital role in the research of LC/aqueous interfaces, the lack of sufficient accuracy in the detection of the target greatly limits the development of LC sensing systems. Therefore, the study of new LC sensing interfaces is valuable to the research and application of LC sensing technology.

Recently, a new LC microarray (LCM) sensing interface combining the birefringence of LCs and the highly ordered microporous structure and unique optical property of inverse opal photonic crystals (IOPhCs) has been designed for the first time and reported by our group.[15] The optical properties of photonic crystals (PhCs) originate from the alternate ordered arrangement of two materials with different refractive indexes, and can be regulated by particle spacing or the refractive index of the material.[16] Therefore, the optical properties of LCM films based on PhCs can be controlled by a change in the refractive index of the LC resulting from an orientation change of the LC molecules, and the optical signals can be recorded in the reflection spectrum. Based on the conformation change of an aptamer adsorbed on the LCM films, the LCM sensor can realize the detection of targets using the change of the reflection peak intensities *via* this novel micro-spectral mode. But the decreased intensity of the reflection peaks is not conducive to the improvement of the observation sensitivity and the identification of optical signals with the naked eye. Therefore, the design of an LCM responsive interface with signal-on output signals is very significant to the development of the LCM sensing method.

Aflatoxins, produced by molds such as *Aspergillus flavus* and *Aspergillus parasiticus*, have attracted increasing attention in the food safety field.[17–19] Among all of the aflatoxins, aflatoxin B1 (AFB1) is identified as the most potent toxic form and one of the strongest known natural carcinogens.[20,21] As a class of naturally occurring carcinogen classified by the World Health Organization, aflatoxins possess high toxicity and can cause great damage to the body (*e.g.*, liver injury, esophageal cancer, and so on),[22] and the maximum tolerance limit of AFB1 is controlled as 0.05–20 ng mL^{-1} according to the Food Hygiene Standards.[23] Though several methods have been developed for the rapid and highly sensitive detection of AFB1,[24–29] they always need expensive instruments and complex signal making processes. Compared with these sensors for the detection of AFB1, the LCM sensor does not need complicated detection processes or instruments; also the LCM sensing interface can be reused, which provides more possibility for the visual detection of AFB1 in real samples.

Herein, a signal-on LCM biosensor is developed using an LCM interface fabricated from inverse opal LC polymer (IO-LCP)

State Key Laboratory of Chemo/Biosensing and Chemometrics, College of Chemistry and Chemical Engineering, Hunan University, Changsha, 410082, P. R. China. E-mail: zywu@hnu.edu.cn, chenqians3@hnu.edu.cn

† Electronic supplementary information (ESI) available: Experimental section, Fig. S1–S7, and Tables S1–S3. See DOI: 10.1039/d2cc00988a

films and LC molecules. According to the induction mechanism of ssDNA for LC molecules in LCM films,[15] an LCM biosensor with a signal-on strategy is designed through the release of ssDNA from $dsDNA_{AFB1}$ driven by the addition of AFB1. The released ssDNA will induce 5CB in the LCM films to convert from the disordered to the ordered arrangement, and clear optical signals were observed in the LCM films by the naked eye. By recording the optical signals using a fiber optic spectrometer and analyzing the intensity of the reflection peaks, the LCM biosensor can realize the quantitative analysis of the target (AFB1). Furthermore, the Partial Response Mechanism (PRM) is proposed for the induction process of ssDNA towards LC molecules, which provides a new vision and a deep understanding of the response mechanism of ssDNA on the LCM surface.

Different from the traditional LC sensing interface, the LCM sensing interface is based on the microporous structure of IOPhCs, and the preparation process is shown in Fig. 1a. Firstly, a 3D ordered PhC array is prepared by the vertical deposition of SiO_2 particles (280 nm) on a glass substrate. Then, the prepolymer composed of the monomers AO6CB and AA, the crosslinker C716 and the initiator HMPP (the mole ratio is 3 : 1 : 1 : 0.05) is infiltrated into the PhC template and further polymerized under UV light to obtain LCP films. After that, IO-LCP films are obtained after etching the LCP films with the PhC templates in HF solution for 5 minutes. As shown in Fig. 1bII, the ordered porous structure of the IO-LCP films has an obvious hexagonal structure that is originated from the PhC template with a face-centered cubic structure, as shown in Fig. 1bI. Additionally, the SEM image of the cross-section of an IO-LCP film (Fig. 1bIII) also shows an ordered 3D porous structure, which demonstrated that the PhC ordered structure has been successfully retained in the IO-LCP films.

Due to the hydrophobicity of AO6CB and the high cross-linker degree of the LCP films, the microporous structure of the IO-LCP films can steadily stabilize in water without swelling and have a great porous structure in air without collapse, which provides favourable conditions for the infiltration of LC molecules into the IO-LCP films. After the preparation of the IO-LCP films, LC molecules in an isotropic state are infiltrated into the porous structure of the film, and an LCM sensing interface based on the LCM film is also developed. As demonstrated in Fig S1 (ESI†), the IO-LCP films have obvious diffractive peaks and the LCM films exhibit no optical signals. This is because the optical properties of PhCs are based on the alternate refractive index in the periodically ordered structure. But when the LC molecules are infiltrated into the structure of the IO-LCP films, the order of the PhCs is broken by the random refractive index caused by the random arrangement of the LC molecules. Therefore, the real images of the IO-LCP films in Fig. S2 (ESI†) show bright green color, and the LCM films appear opaque white. This also provides a clear color comparison for the response of ssDNA.

As proven in a previous study, the optical properties of LCM films can be modulated by single-stranded nucleic acid (ssDNA) but not double-stranded nucleic acid (dsDNA).[15] This is because the exposed base groups of ssDNA have an interaction force with the cyano groups of the LC molecules (5CB), and this interaction force changes the orientation of the LC molecules from disordered to ordered. According to the physical properties of the LCs, the ordered LC molecules have a uniform refractive index, which satisfies the conditions required for Bragg diffraction of the PhCs. Therefore, the optical properties of the LCM films based on the IOPhC structure will be changed by the change of the LC molecule arrangement. Using this response mechanism, a signal-on strategy based on LCM films is developed for the detection of AFB1, and the schematic diagram is shown in Fig. S3 (ESI†).

Specifically, the $dsDNA_{AFB1}$ contained C_{AFB1} and the $C_{c\text{-}AFB1}$ is designed to realize the release of $C_{c\text{-}AFB1}$ after AFB1 combines with the aptamer C_{AFB1}. Due to the lack of exposed base groups of $dsDNA_{AFB1}$, the $dsDNA_{AFB1}$ will not change the disordered arrangement of the LC molecules in the LC films and modulate the optical properties of the LCM films. As demonstrated in Fig. S4 (ESI†), the LCM films that reacted with $dsDNA_{AFB1}$ do not have optical signals, indicating that the 5CB in the LCM films has no response to $dsDNA_{AFB1}$. After the addition of AFB1, the C_{AFB1} specifically binds to AFB1 and $C_{c\text{-}AFB1}$ is released into the solution as ssDNA. These free $C_{c\text{-}AFB1}$ will interact with 5CB in the LCM films and the orientation of the LC molecules changes from the disordered to the ordered arrangement, and the optical properties of the LCM films will be regulated and the diffraction peaks can be recorded by a micro-spectral optical fiber. As shown in Fig. S5a (ESI†), the reflection peak of the LCM films is observed clearly when AFB1 is present, which suggests that the optical signal of the LCM films is controlled by the released $C_{c\text{-}AFB1}$, and the orientation of the LC molecules is also changed from the disordered to ordered arrangement. This result shows that the signal-on strategy is successfully applied to the LCM sensing system.

Beyond that, this response mechanism is further investigated using the fluorescent optical images (FOM), polarized optical images (POM), and circular dichroism spectrum (CDS). In Fig. S5b (ESI†), the FOM has distinct fluorescent signals only when the target is present, which resulted from the fluorescent labels of $C_{c\text{-}AFB1}$ that are adsorbed on the surface of the LCM films. In addition, the initial optical appearance of the LC images turns black due to the addition of AFB1, which means

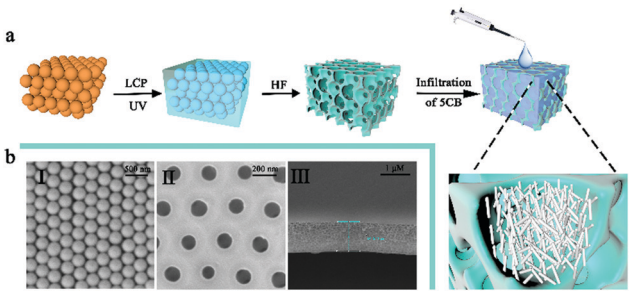

Fig. 1 (a) The fabrication process of the LCM films and a schematic diagram of the LC molecules in the LCM films, shown by the amplified section in the bottom right corner. (b) The SEM images. SEM image I is a surface image of the SiO_2 PhC template, SEM image II is a surface image of an IO-LCP film, and SEM image III is a sectional view of an IO-LCP film. The scale bars are 500 nm, 200 nm and 2 μm, respectively.

an ordered orientation of the LC molecules that is perpendicular to the aqueous–LC surface. These results prove that the $C_{c\text{-}AFB1}$ is released into the solution, and further adsorbs on the surface of the LCM films by the interaction of the base groups in the ssDNA and the cyano groups in 5CB. Thus, 5CB is induced by $C_{c\text{-}AFB1}$ to convert from the disordered to the ordered arrangement, and the optical properties of the LCM films are changed. Furthermore, the intensity of the CDS of the responsive solution exhibits a significant decrease after the addition of the target, as shown in Fig. S5c (ESI†), which shows that the amount of dsDNA is reduced due to the specific binding of C_{AFB1} to AFB1. And because the free $C_{c\text{-}AFB1}$ is mainly adsorbed on the surface of the LCM films, there is no characteristic peak of ssDNA, which further confirms the successful preparation of the LCM biosensor.

To improve the binding efficiency of the aptamer and AFB1, the complementary chain $C_{c\text{-}AFB1}$ with different base groups (C14–C24) is used to form $dsDNA_{AFB1}$ and the responsivity to AFB1 is further examined. Firstly, it is demonstrated in Fig. S4 (ESI†) that none of these $dsDNA_{AFB1}$ with different numbers of base groups in $C_{c\text{-}AFB1}$ exhibit significant reflection peaks, which is consistent with the results in the above responsiveness experiments. Furthermore, the change of the reflection peak intensity in Fig. S5d and e (ESI†) shows that the change in intensity increases with a decrease in the number of base groups in $C_{c\text{-}AFB1}$ and reaches the maximum when C14 is used in $dsDNA_{AFB1}$. This result means that the LCM biosensor has the best response to AFB1 when C14 is used as $C_{c\text{-}AFB1}$. This is because, with the reduction of the number of base groups in $C_{c\text{-}AFB1}$, the C_{AFB1} has more exposed base groups and more easily binds with AFB1, so the amount of released $C_{c\text{-}AFB1}$ is increased and the $C_{c\text{-}AFB1}$ further induces the 5CB in the LCM films. This is also proved in the fluorescence experiments shown in Fig. S5f (ESI†), where the fluorescence intensity of dsDNA is decreased with the decrease of the number of base groups in $C_{c\text{-}AFB1}$ after the dsDNA dyed by SYBR Green I reacts with AFB1. Because the fluorescence signals are originated from the specific binding between SYBR Green I and double bonds, the constant decrease in fluorescence intensity signifies that the amount of dsDNA is gradually reduced with the increase in the binding efficiency between the aptamer and AFB1. Thus, C14 is used for the subsequent experiments for the best response of the LCM biosensor to AFB1. It is noted that complementary ssDNA with lower base numbers (such as C12 and C10) is not used in this paper because the $dsDNA_{AFB1}$ (D12 or D10) has some interference with the interaction of 5CB and the optical signal of the LCM films due to the exposed base groups in the aptamer. Additionally, other influencing factors (pH value, the concentration ratio of $C_{c\text{-}AFB1}$ and C_{AFB1}, temperature) of the LCM biosensors for the detection of AFB1 are also studied (Fig. S6, ESI†).

Under the optimization conditions, the determination ability of the LCM biosensor is further investigated (Fig. 2). The results show that the LCM biosensor has a great response ability to AFB1 in the range of 300 pM to 200 μM. And the change in the reflection peak intensity and the logarithm of concentration exhibit a good linear relation in the range from

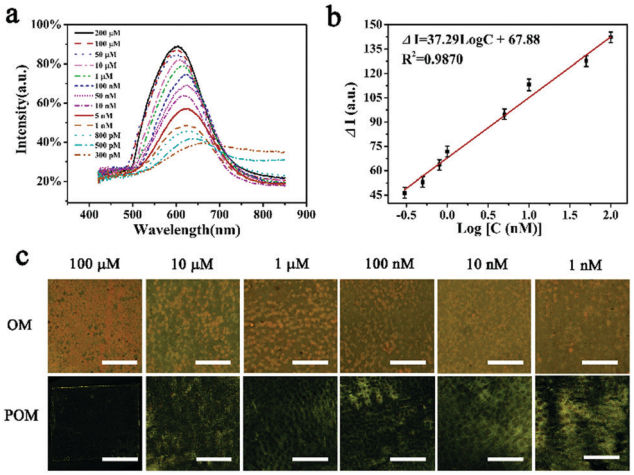

Fig. 2 The detection of the LCM biosensor toward AFB1. (a) The reflection peaks of the LCM films after the detection to AFB1 with different concentrations. (b) The linear relationship of the reflection peak intensity and AFB1 concentration from 300 pM to 100 nM. The error bars indicate the deviation for three assays. (c) The OM and POM in the range from 1 nM to 100 μM. The scale bars are 200 nm.

300 pM to 100 nM with the R^2 being 0.9870 (Fig. 2b). This result is lower than the detection standard in many countries, which shows that this signal-on LCM biosensor has good detection performance towards AFB1. Different optical detection methods are compared with the LCM biosensor in Table S2 (ESI†). Although the detection result is not the lowest of these sensors, the fabrication and detection of the LCM sensor do not need extra labels, or expensive and sophisticated instruments, possessing good practical prospects in the preliminary detection of AFB1.

At the same time, optical images (OM) and POM of the LCM films were captured in the detection process (Fig. 2c). It is worth noting that some bright spots are observed in the POMs with a lower concentration of AFB1, and the number of spots gradually reduces with an increase in the AFB1 concentration and it finally becomes uniform black when the concentration exceeds 100 μM. This phenomenon is very exciting because it shows a clearer response process for the modulation of the optical properties of the LCM films. With the gradual change of the responsive areas, a schematic diagram is presented (Fig. 3) to describe this response mechanism, named the Partial Response Mechanism (PSM). To be specific, this is a response process of LC molecules (5CB) to ssDNA from local to whole parts, which may be attributed to the low concentration of ssDNA (C14) released from the dsDNA. Because it is limited by the binding efficiency of the aptamer and AFB1, the number of C14 molecules required to induce 5CB from the disordered to the ordered arrangement is less than the released amount of ssDNA calculated in theory. Simultaneously, given the weak interfacial interaction of ssDNA and 5CB, the response areas are not evenly distributed on the interface of the LCM films when the content of ssDNA is low. Thus, these responsive areas are distinctly observed in the POMs (bright spots) and OMs (red spots). The PSM not only clearly explains the responsiveness process of 5CB in the LCM films to ssDNA, but also

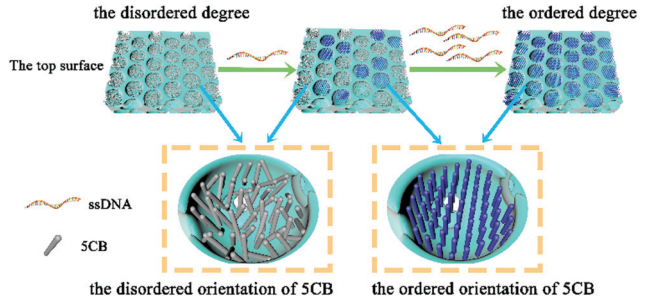

Fig. 3 A schematic diagram of the Partial Response Mechanism (PSM) of the LCM biosensor. With the increase of the amount of ssDNA, the response area is changed from partial to whole, and the ordered degree of orientation of the LC molecules is also increased. An enlarged view of LCM films with disordered degree and ordered degree is shown in the dotted boxes.

provides sufficient conditions to further deeply explore the modulation mechanism of the optical properties of the LCM films, which is of vital significance to the development of LC microarray sensing systems.

To verify the specificity of the LCM biosensor to AFB1, some common interfering substances (AFB2, AFG1, OTA, OTB, FB1, and ZAE) are selected due to their similar chemical structure. These substances were added into $dsDNA_{AFB1}$ solution, respectively, and induced LC molecules in LCM films under the same detection conditions as AFB1. As demonstrated in Fig. S7 (ESI†), only the addition of AFB1 results in the increase of the intensity of the reflection peaks, which shows that 5CB in the LCM films exhibits no response to the other substances tested, even though they have a similar structure to AFB1. This is because the ssDNA (C14) is released only when the C_{AFB1} binds to AFB1 due to the specific identification ability. This result indicates that the LCM biosensor has great selectivity to AFB1 because of the specific binding between the aptamer and AFB1, which also provides conducive conditions for detection in real samples.

AFB1 is always found in corn, soybean, rice, wine, and cooking oil, and the detection of AFB1 in real samples is of important significance to food safety and body health. Herein, 10-fold diluted corn flour and beer samples are used as actual samples for the detection of AFB1 using the standard addition method, and the results of the recovery test are shown in Table S3 (ESI†). As demonstrated in the results, the LCM biosensor shows good response performance in actual samples, which provides a new detection platform for AFB1 in the food field.

In summary, a LCM biosensor based on the signal-on optical signal strategy for the detection of AFB1 has been developed. Using the specific binding of the aptamer and AFB1, the complementary ssDNA is successfully released and induces the LC molecules in the LCM films to change from the disordered to ordered orientation arrangement. Meanwhile, the LCM biosensor realizes the quantitative analysis of AFB1 in the range of 300 pM to 100 nM utilizing the novel microspectral optical sensing signals. More importantly, the response mechanism, PSM, is proposed for the first time and discussed in the LCM sensing system, which is beneficial to clearly understanding and explaining the induction process of ssDNA towards LC molecules. At the same time, an in-depth study of this mechanism will provide great prospects for the design and development of LCM sensing platforms.

This study was financially supported by the National Natural Science Foundation of China (21874037 and 21675045), and the Postdoctoral Science Foundation of China (2021M701148).

Conflicts of interest

There are no conflicts to declare.

Notes and references

1 C. L. Luan, H. P. Luan and D. W. Luo, *Micromachines*, 2020, **11**, 19.
2 Z. Hussain, F. Qazi, M. I. Ahmed, A. Usman, A. Riaz and A. D. Abbasi, *Biosens. Bioelectron.*, 2016, **85**, 110–127.
3 R. J. Carlton, J. K. Gupta, C. L. Swift and N. L. Abbott, *Langmuir*, 2012, **28**, 31–36.
4 D. Y. Zhao, Y. Peng, L. H. Xu, W. Zhou, Q. Wang and L. Guo, *ACS Appl. Mater. Interfaces*, 2015, **7**, 23418.
5 X. X. Yang, H. Y. Li, X. F. Zhao, W. Liao, C. X. Zhang and Z. Q. Yang, *Chem. Commun.*, 2020, **56**, 5441–5444.
6 M. Tsuei, M. Shivrayan, Y. K. Kim, S. Thayumanavan and N. L. Abbott, *J. Am. Chem. Soc.*, 2020, **142**, 6139–6148.
7 X. G. Wang, P. Yang, F. Mondiot, Y. X. Li, D. S. Miller, Z. Chen and N. L. Abbott, *Chem. Commun.*, 2015, **51**, 16844–16847.
8 B. H. Clare, O. Guzman, J. de Pablo and N. L. Abbott, *Langmuir*, 2006, **22**, 7776–7782.
9 H. Tan, X. Li, S. Z. Liao, R. Q. Yu and Z. Y. Wu, *Biosens. Bioelectron.*, 2014, **62**, 84–89.
10 J. Shen, F. J. He, L. C. Chen, L. Ding, H. L. Liu, Y. Wang and X. L. Xiong, *Microchim. Acta*, 2017, **184**, 3137–3144.
11 L. B. Qi, S. Y. Liu, Y. F. Jiang, J. M. Lin, L. Yu and Q. Z. Hu, *Anal. Chem.*, 2020, **92**, 3867–3873.
12 W. W. Li, K. Mashooq and L. Lin, *Angew. Chem., Int. Ed.*, 2020, **59**, 9282–9287.
13 I. Verma, M. Devi, D. Sharma, R. Nandi and S. K. Pal, *Langmuir*, 2019, **35**, 7816–7823.
14 M. Sadati, H. Ramezani-Dakhel, W. Bu, E. Sevgen, Z. Liang, C. Erol, M. Rahimi, N. T. Qazvin, B. H. Lin, N. L. Abbott, B. Roux, M. L. Schlossman and J. J. De Pablo, *J. Am. Chem. Soc.*, 2017, **139**, 3841–3850.
15 S. H. Wang, Y. Qi, Q. S. Chen, G. N. Zhang, B. Liu, F. B. Xiao, J. Zhou, Z. Y. Wu and R. Q. Yu, *Anal. Chem.*, 2021, **93**, 11887–11895.
16 M. L. T. Cossio, L. F. Giesen, G. Araya, M. L. S. PérezCotapos, R. L. Vergara, M. Manca, R. A. Tohme, S. D. Holmberg, T. Bressmann and D. R. Lirio, *Photonic crystals: Molding the Flow of Light*, 2013.
17 M. Twaruzek, P. Skrzydlewski, R. Kosicki and J. Grajewski, *Toxicon*, 2021, **202**, 27–39.
18 J. Janicki, K. Szebiotko, M. Kokorniak, M. Wiewiorowska, J. Chelkowski and B. Godlewska, *Die Nahrung*, 1974, **18**, 27–37.
19 M. Abrar, F. M. Anjum, M. S. Butt, I. Pasha, M. A. Randhawa, F. Saeed and K. Waqas, *Crit. Rev. Food Sci. Nutr.*, 2013, **53**, 862–874.
20 G. Suarez Fernandez and M. Ylla-Catala Genis, *Pharm. Acta Helv.*, 1979, **54**, 78–81.
21 S. K. Altun, F. Temamogullari, A. Yigin and S. Gurbuz, *Fresenius Environ. Bull.*, 2019, **28**, 6644–6650.
22 D. Schrenk, M. Bignami and L. Bodin, *EFSA J.*, 2020, **18**, 112.
23 E. Janik, M. Niemcewicz, M. Ceremuga, M. Stela, J. Saluk-Bijak, A. Siadkowski and M. Bijak, *Int. J. Mol. Sci.*, 2020, **21**, 21.
24 R. M. Gell and I. Carbone, *J. Microbiol. Methods*, 2019, **158**, 14–17.
25 R. Liu, W. Li, T. T. Cai, Y. Deng, Z. Ding, Y. Liu, X. R. Zhu, X. Wang, J. Liu, B. W. Liang, T. S. Zheng and J. L. Li, *ACS Appl. Mater. Interfaces*, 2018, **10**, 14447–14453.
26 T. H. Jiao, W. Ahmad, J. J. Zhu, M. M. Hassan, J. J. Wang, Y. W. Rong, Z. M. Guo, H. H. Li, Z. Ding, C. X. Lv and Q. S. Chen, *Sens. Actuators, B*, 2021, **331**, 129424.
27 X. H. Xiong, Y. F. Li, W. Yuan, Y. C. Lu, X. Xiong, Y. Li, X. Y. Chen and Y. J. Liu, *Biosens. Bioelectron.*, 2020, **150**, 6.
28 J. Pietschmann, H. Spiegel, H. J. Krause, S. Schillberg and F. Schroper, *Toxins*, 2020, **12**, 15.
29 C. X. Zhu, D. Liu, Y. Y. Li, S. Ma, M. Wang and T. Y. You, *Biosens. Bioelectron.*, 2020, **174**, 112654.

